

## Recent advancement in the study of Performance Comparision of horn antenna loaded viaDNG Metamaterial

Ritesh Kumar Kushwaha<sup>1</sup>, Sanjay Srivastava<sup>2</sup>, Yogesh Srivastava<sup>2</sup>

<sup>1</sup>*Department of Electronics & Communication, Petal Group of Institution, Bhopal, (M.P), India*

<sup>2</sup>*Department of Materials Science and Metallurgical Engineering, Maulana Azad National Institute of Technology, Bhopal (M.P.), India*

**Abstract:** Now-a-days metamaterials or Double Negative Gain (DNG) Structure have been widely used due to its potential applications. They are usually arranged in periodic patterns and gain properties not from their composition, but from their exacntly-designed structures. In this paper we report the detailed design and theoretical demonstration of the Split Ring Resonator (SRR), Metellic strip wires (SW) to develop metamaterials which has been loaded on pyramidal horn antenna for X-band application . The obtained result from the HFSS simulation concerning the constitutive parameters of the SRR, shows that there is a DNG permeability and permittivity in the frequency of interest. The horn antenna is loaded with fabricated DNG structure and various parameters have been measured at operating frequency of 8.5 GHz and 10 GHz. It was found that the results are improved at 8.5 GHz as compared to that of unloaded condition, while at 10 GHz DNG structure worked as normal material but the rate of performance of horn antenna decreases.

**Keywords:** DNG, Metamaterial, Pyramidal horn, SRR, SW, X-Band.

---

### I. Introduction

The horn-reflector antenna was selected for the satellite for the communication satellite that relay television and radio signals, telephone calls and data around the worldground station of its broadband and low-noise properties along with certain operational advantages. Two commonly used microwave bands on satellites are C-band used for long-distance radio and telecommunications and Ku-band used for broadcast television and remote television uplinks. The pyramidal horn is widely used as a standard gain horn, as a feed for reflector and as an element in phase array antennas due to its such salient features as high gain, moderate bandwidth, construction simplicity, good power handling capability and low fabrication cost [1-4]. To make the pyramidal horn more compact, several approaches that include lens-correction [5-7] and dielectric loading [8, 9] have been considered. An important antenna design requirement is a wide impedance bandwidth.

Horn antennas loaded with dielectrics or ferrite materials [10], have desirable properties such as increaseddirectivity, reduced side lobe level, wide bandwidth, low loss, and ease of fabrication [11, 12]. These properties are particularly attractive for applications such as ultra-wideband (UWB) ground penetrating radars (GPR) [13, 14]. Electronic devices utilizing antennas are limited in physical size as determined by the size of the incorporated antenna. The characteristic dimensions of the antennas are directly proportional to their operation wavelength ( $\lambda$ ) and for efficient radiation and  $\lambda/2$  for should be the effective length of the electrical sizes. The introduction of the so-called meta-materials (MTMs), artificial materials which have engineered electromagnetic responses, and their exotic properties have provided an alternate design approach that hasled to improved performance characteristics of several radiating and scattering systems [15]. Left-handed meta-materials (LHMs) are an artificial periodic structure, whose effective permittivity and permeability are simultaneously less than zero [16]. The term “left-handed” has been used for such a medium, in which the vectors  $E$ ,  $H$  and  $K$  form a left-handed triplet, and the energy propagates in a direction opposite to that of the phase velocity. So many peculiar electromagnetic properties occur, such as negative refraction [17], reversed Doppler shift [18], perfect lens [19], etc. The initial analytical research into the meta-material-based EESA (efficient electrically small antenna) systems given in [20, 21] revealed that it is possible to design an EESA system formed by an electrically small electric dipole antenna radiating in the presence of either an idealized homogeneous and isotropic double-negative (DNG) spherical shell. As a special periodic structure, the reflection of LHMs may widen their applications. Generally,  $\epsilon$  and  $\mu$  are both positive for ordinary materials. However, by taking advantage of artificially constructed periodic structures, one can have negative values of  $\epsilon$  and  $\mu$ . The accepted power (AP) in EESA is the power delivered to the antenna terminals from the source. It contains information about any mismatch between the source, the feedline, and the antenna. Let  $P_{input}$  be the input power of the source. Let  $Z_0$  be the characteristic impedance of both the source and the feedline, i.e., assume that the feedline is matched to the source. Let  $Z_{input}$  be the input impedance of the antenna. The reflection coefficient at the antenna is  $\Gamma = (Z_{input} - Z_0)/(Z_{input} + Z_0)$  and the accepted power by the antenna is then  $AP = (1 - |\Gamma|^2) P_{input}$ , where

the mismatch or accepted power efficiency  $A_E = AP/1 - |\Gamma|^2$ . The radiation efficiency is the ratio of the total power radiated to the accepted power, i.e.,  $RE = P_{rad}/AP$ .

Two common methods are used to obtain the effective parameters of a MM: the  $S$ -parameter retrieval [22] and the field averaging method [23]. The first is based on measuring (or calculating) the  $S$  parameters ( $S_{11}$ , reflection and  $S_{21}$ , transmission) of a MM slab, assuming they correspond to a homogeneous slab and then using analytical inversion to find  $\epsilon$  and  $\mu$  from  $S_{11}$  and  $S_{21}$ . In the field averaging method, the  $E$  and  $H$  fields of propagating (Bloch) modes in an infinite MM are numerically calculated while effective  $\epsilon$  and  $\mu$  are found by averaging the fields over a unit cell. In spectral regions where EM fields are not allowed to propagate (band gaps), one has to find the complex Bloch bands [24] to obtain  $\epsilon$  and  $\mu$ . With the exception of [25-27], studies reported so far (numerical or experimental) assume the EM wave falling perpendicularly on the MM surface. Scalar  $\epsilon$  and  $\mu$  obtained for perpendicular incidence cannot a priori be used for other angles because they do not account for (bi) anisotropy. Also, since MMs are operated in a regime where the wavelength is at most one order of magnitude larger than the unit cell, there is no a priori reason why the effective parameters would be angle-independent.

Meta-material superstrate composed of stacked S-shaped split ring resonators were used for the design of WiMAX 2.5 GHz band (2.50-2.69 GHz) [28]. Regarding the  $E$ -plane horn antenna design, numerical methods involving geometrical diffraction theory and conventional aperture techniques were employed to analyze the radiation characteristics of  $E$ -plane horn antennas [29-31]. The radiation patterns of rectangular electromagnetic horn antennas against the structural parameters such as flare angle and radial length were systematically used for the design of pyramidal horn antenna [32]. A reflection of diffracted fields from the horn interior and double diffraction at the aperture were considered to explain the gain variation observed in a pyramidal horn antenna [33, 34]. Recently, several novel horn antennas of new type's geometry were designed and analyzed such as compound box-horn antenna and modified TEM horn antenna [35, 36]. The former one showed the advantages of both the modified box-horn and pyramidal horn antennas whereas the latter one removed fluctuations introduced by conventional TEM horn antenna by carving an arc shape on the antenna's open end.

The present study is organized as follows. In Section I presents the basic concept of the geometry and the operational principle of pyramidal horn and DNG meta-material. In Section II presents Fabrication and Testing of pyramidal Horn and pyramidal Horn loaded with DNG. In Section IV we describe the results of experiments within the computing environment HFSS V.10, which is based on finite element method (FEM) while Section V contains the conclusions and working deductions.

## **II. Operational Principle And Geometry Of A Horn Antenna**

An antenna may be considered as transformer from the impedance of a transmission line to the impedance of the free space, 377 ohms. A common microwave transmission line is waveguide, a hollow pipe carrying an electromagnetic wave. If one dimension of the pipe is greater than a half wavelength, then the wave can propagate through the waveguide with extremely low loss. And if the end of a waveguide is simply left open, the wave will radiate out from the open end.

Horn antennas are of aperture antennas class, directed radiation of which is formed by a flat opening  $S$  surface. The simplest aperture antenna appears to be open end of a waveguide, though due to relatively small size of radiating aperture against a wavelength  $\lambda$ , such antenna has a weak directivity. Improvement of the latter can be achieved by a gradual extension of the opening size, due to which waveguide transforms into a horn antenna. A horn antenna flared in a plane of the magnetic field  $H$  is called an  $H$ -plane sectoral horn. A horn flared in the plane of the electric field  $E$  is called an  $E$ -plane sectoral horn. A horn flared in both the  $E$  and  $H$  planes is called a pyramidal horn. The typical figure of horn antenna is shown in Figure 1.

Figure 2 shows the geometry of the horn antenna in more detail. The two lower figures are the cross-sectional views along the  $xz$ - and  $yz$ -planes. It follows from the geometry that the various lengths and flare angles are given by

$$R_a = \frac{A}{A-a} R_A \quad R_b = \frac{B}{B-b} R_B \quad (1)$$

$$L_a^2 = R_a^2 + \frac{A^2}{4} \quad L_b^2 = R_b^2 + \frac{B^2}{4} \quad (2)$$

$$\tan \alpha = \frac{A}{2R_a}, \tan \beta = \frac{B}{2R_b} \quad (3)$$

$$\Delta_a = \frac{a^2}{8R_a}, \Delta_b = \frac{B^2}{8R_b} \quad (4)$$

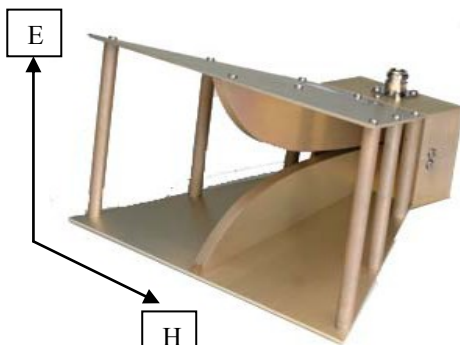


Fig.1.Pyramidal Horn Antenna

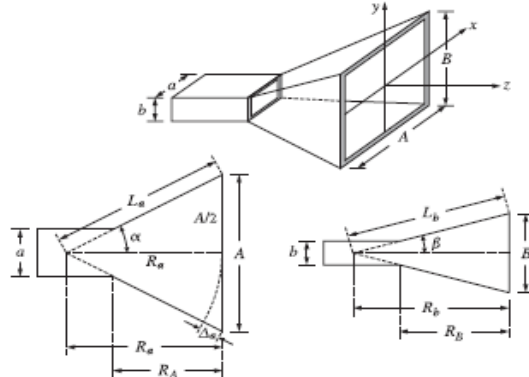


Fig.2.Geometry of the Horn Antenna

The quantities  $R_A$  and  $R_B$  represent the perpendicular distances from the plane of the waveguide opening to the plane of the horn. Therefore, they must be equal,  $R_A = R_B$ . Given the horn sides A, B and the common length  $R_A$  (given by equation 1) allow the calculation of all the relevant geometrical quantities required for the construction of the horn. The lengths  $\Delta_a$  and  $\Delta_b$  represent the maximum deviation of the radial distance from the plane of the horn. The expressions given in 6 are approximations obtained when  $R_a \gg A$  and  $R_b \gg B$ . Indeed, using the small -  $x$  expansion,

$$\sqrt{1 \pm x} \approx 1 \pm \frac{x}{2} \quad (5)$$

By using this expression, the following parameters are evaluated:

$$\begin{aligned} \Delta_a &= L_a - R_a = \sqrt{R_a^2 + \frac{A^2}{4}} - R_a \approx \frac{A^2}{8R_a} \\ &= L_a - \sqrt{L_a^2 - \frac{A^2}{4}} = L_a - L_a \sqrt{1 - \frac{A^2}{4L_a^2}} \approx \frac{A^2}{8L_a} \end{aligned} \quad (6)$$

The two expressions are equal within the assumed approximation order. The length  $\Delta_a$  is the maximum deviation of the radial distance at the edge of the horn plane, that is, at  $x = \pm A/2$ . For any other distance  $x$  along the A-side of the horn, and distance  $y$  along the B-side, the deviations will be:

$$\Delta_a(x) = \frac{x^2}{2R_a}, \Delta_a(y) = \frac{y^2}{2R_b} \quad (7)$$

The quantities  $k\Delta_a(x)$  and  $k\Delta_b(y)$  are the relative phase differences at the point  $(x, y)$  on the aperture of the horn relative to the center of the aperture. To account for these phase differences, the aperture electric field is assumed to have the form:

$$E_y(x, y) = E_o \cos\left(\frac{\pi x}{A}\right) e^{-jk\Delta_a(x)} e^{-jk\Delta_b(y)} \quad (8)$$

Or

$$E_y(x, y) = E_o \cos\left(\frac{\pi x}{A}\right) e^{-jk\Delta_a(x)} e^{-jk\Delta_b(y)} \quad (9)$$

We have noticed that at the connecting end of the waveguide the electric field is  $E_y(x, y) = E_o \cos\left(\frac{\pi x}{A}\right)$

and changes gradually into the form of (9) at the horn end. Because the aperture sides A, B are assumed to be large compared to  $\lambda$ , the Huygens source assumption is fairly accurate in the tangential aperture magnetic field

$$H_x(x, y) = -\frac{1}{\eta} E_y(x, y), \text{ so that:}$$

$$H_x(x, y) = -\frac{1}{\eta} E_y \cos\left(\frac{\pi x}{A}\right) e^{-jkx^2/2R_a} e^{-jky^2/2R_b} \quad (10)$$

The quantities  $k\Delta_a$ ,  $k\Delta_b$  is the maximum phase deviations in radians. Therefore,  $\Delta_a/\lambda$  and  $\Delta_b/\lambda$  will be the maximum deviations in cycles. We define the following quantities :

$$S_a = \frac{\Delta_a}{\lambda} = \frac{A^2}{8\lambda R_a}, \quad S_b = \frac{\Delta_b}{\lambda} = \frac{B^2}{8\lambda R_b} \quad (11)$$

It turns out that the optimum values of these parameters that result into the highest directivity are approximately:  $S_a = 3/8$  and  $S_b = 1/4$ . For the purpose of deriving convenient expressions for the radiation patterns of the horn, we define the related quantities:

$$\sigma_a^2 = 4S_a = \frac{A^2}{2\lambda R_a}, \quad \sigma_b^2 = 4S_b = \frac{A^2}{2\lambda R_b} \quad (12)$$

The near-optimum values of these constants are  $\sigma_a = \sqrt{4S_a} = \sqrt{4(3/8)} = 1.2247$  and  $\sigma_b = \sqrt{4S_b} = \sqrt{4(1/4)} = 1$ . These are used very widely, but they are not quite the true optimum values, which are  $\sigma_a = 1.2593$  and  $\sigma_b = 1.0246$ . Replacing  $k = \frac{2\pi}{\lambda}$  and  $2\lambda R_a = \frac{A^2}{\sigma_a^2}$  and  $2\lambda R_b = \frac{B^2}{\sigma_b^2}$  in (9), we may rewrite the aperture fields in the form: For  $-A/2 \leq x \leq A/2$  and  $-B/2 \leq y \leq B/2$ ,

$$E_y(x, y) = E_o \cos\left(\frac{\pi x}{A}\right) e^{-j\left(\frac{\pi}{2}\right)\sigma_a^2\left(\frac{2x^2}{A}\right)} e^{-j\left(\frac{\pi}{2}\right)\sigma_b^2\left(\frac{2y^2}{B}\right)} \quad (13)$$

$$H_x(x, y) = -\frac{1}{\eta} E_o \cos\left(\frac{\pi x}{A}\right) e^{-j\left(\frac{\pi}{2}\right)\sigma_a^2\left(\frac{2x^2}{A}\right)} e^{-j\left(\frac{\pi}{2}\right)\sigma_b^2\left(\frac{2y^2}{B}\right)} \quad (14)$$

The radiated power  $P_{rad}$  is obtained by integrating the Poynting vector of the aperture fields over the horn area.

$$P_{rad} = \frac{1}{4\eta} |E_o|^2 (AB) \quad (15)$$

It follows that the horn directivity will be

$$D = 4\pi \frac{U_{max}}{P_{rad}} = e \frac{4\pi}{\lambda^2} AB \quad (16)$$

Using the optimum values of  $\sigma_a$  and  $\sigma_b$  we obtain the optimum value of  $e$  as 0.49. This transforms the directivity of the horn antenna as

$$D = 0.49 \frac{4\pi}{\lambda^2} AB \quad (19)$$

Some of the other important parameters of the horn antenna are defined below.  
Beam width between first nulls

$$(E - plane) = \frac{115\lambda}{A} \quad (20)$$

Beam width between first nulls

$$(H - plane) = \frac{172\lambda}{A} \quad (21)$$

$$\text{Half power beam width } (E - plane) = \frac{56\lambda}{A} \quad (22)$$

$$\text{Half power beam width } (H - plane) = \frac{67\lambda}{A} \quad (23)$$

### III. Fabrication Of The Dng And Horn Annetna

Fabrication of any structure should be preceded by the proper designing of the structure so that the structure meets the requirements. Fabrication of SRR structure and SW structure is carried out separately and then these two structures are combined to form the required DNG structure. Here the dimensions of the DNG structure are taken as:  $l = 3$  mm,  $d = t = g = 0.3$  mm,  $a = 0.5$  mm,  $b = 3$  mm, the spacing between the DNG units is 4 mm as shown in Figure 4.

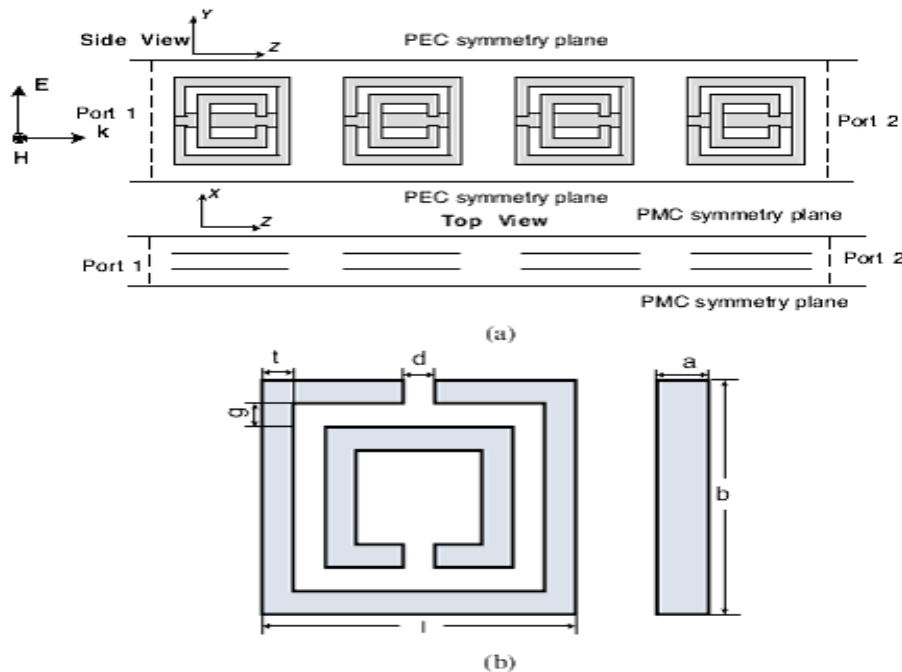


Fig. 4(a) DNG structure geometry, (b) Dimensions of the DNG structure.

Here the unit cell of DNG structure is replicated many times so that the whole DNG structure has a dimension of 10cm\*8cm which is required to completely cover the face of the horn antenna on which testing is done.

The photo of the DNG structure fabricated is shown in Figure 5. The two structures shown above are joined to form the required DNG structure and then the DNG structure is tested in the presence of the horn antenna.

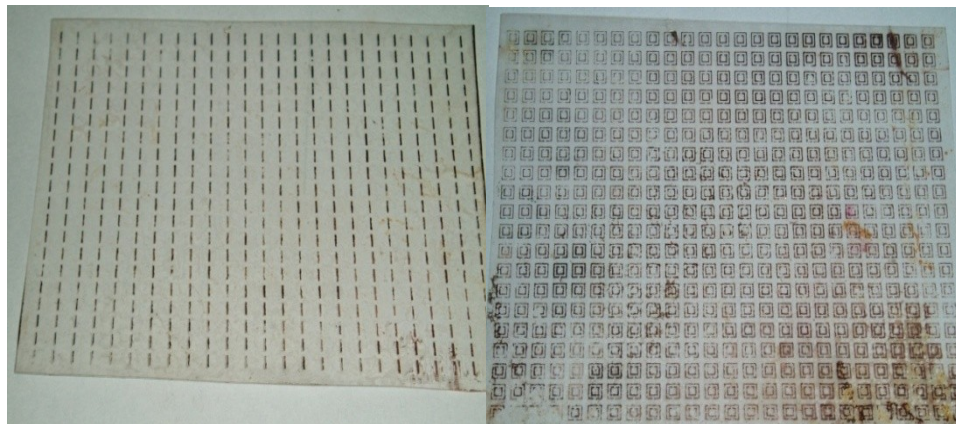


Fig. 5 (a) Strip Wire structure

Fig. 5 (b) Split Ring Resonator structure.

The horn antenna has a dimension of 2.65\*1.944in at the mouth and a dimension of 0.9\*0.4in at the throat of the horn antenna. The horn antenna is enclosed in a radiation boundary of dimension 5in\*4in\*3in. In Figure 6 structures are shown.

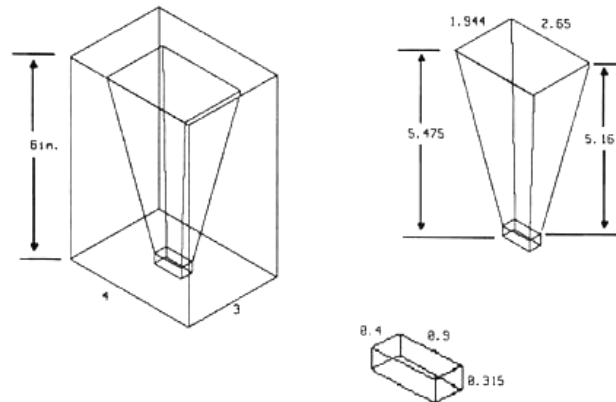


Fig.6 (a) Horn Antenna used for simulation (b) Dimensions of the horn antenna.

## TESTING

Testing is done in two steps. Firstly the horn antenna characteristics without DNG structure are measured. The E – Plane, H – Plane radiation patterns at 8.5GHz and 10GHz frequencies are measured with the experimental setup shown in Figure 7. The E – Plane and H – Plane cross polarization patterns at the two frequencies are also measured with the experimental setup shown in Figure 7. The radiation patterns are plotted with the help of Microsoft Excel software. The horn antenna which is used for testing has the dimensions of 9.6cm\*7.6cm at the mouth and 2.286cm\*1.016cm at the throat. The axial length of the horn antenna is 11.5cm. From this information one will be able to calculate the flare angles.

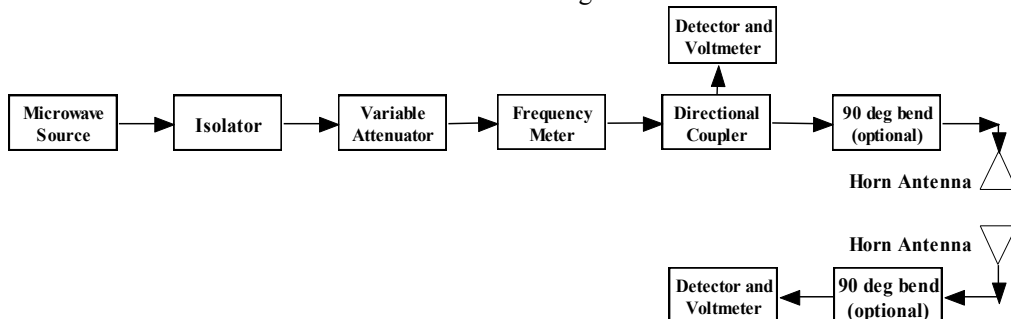


Fig. 7 Laboratory setup for measuring antenna characteristics without DNG structure.

As the gain of the standard antenna is known the gain of our test antenna is calculated using the formula:

$$\frac{G_1}{G_2} = \frac{R_1}{R_2} \quad (24)$$

After the measurement with the standard horn antenna, the standard horn antenna is replaced by the test horn antenna. The DNG structure is placed in front of the horn antenna and the radiation characteristics of the horn antenna are measured with DNG at both 8.5 GHz and 10 GHz, experimental setup shown in Figure 7. The gain of test antenna with DNG is calculated from (24) at both the frequencies.

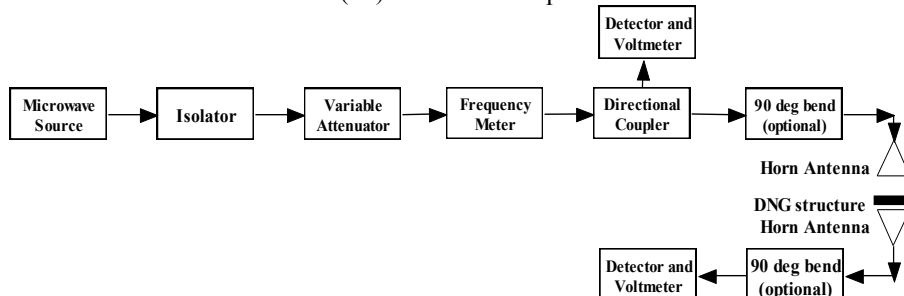


Fig. 8. Laboratory setup for measuring antenna characteristics with DNG structure.

## IV. Result

The magnitude and phase plots of  $S_{11}$  and  $S_{21}$  of the DNG structure are shown in Figure 9 and 10. The effective permittivity and effective permeability are plotted as shown in Figure 11.

Figure9 & 10 shows that the DNG structure produces a passband in which the magnitude of  $S_{21}$  is greater than that of  $S_{11}$ . From Figure 11, it could be understood that this DNG structure is producing effective

negative permittivity and permeability in a passband. There was a peak in the magnitude of  $S_{21}$  curve and a sharp transition in the phase of the  $S_{21}$  curve at the frequencies where the effective permittivity and permeability are simultaneously negative. Because of this extraordinary property of the DNG structure, DNG structure can be applied to an antenna to congregate the incident radiation field. The unit number of the antenna arrays could be reduced for the same gain, which has the greatest significance of the minimization design of the antenna arrays.

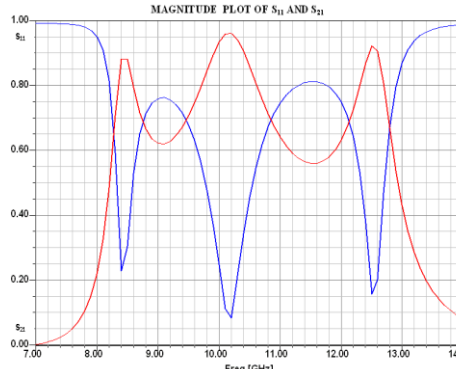


Fig.9. Magnitude plots of  $S_{11}$  and  $S_{21}$ .

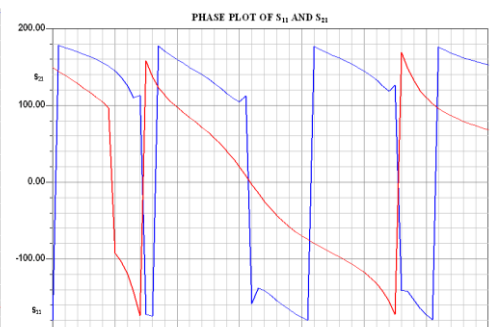


Fig.10. Phase plot of  $S_{11}$  and  $S_{21}$ .

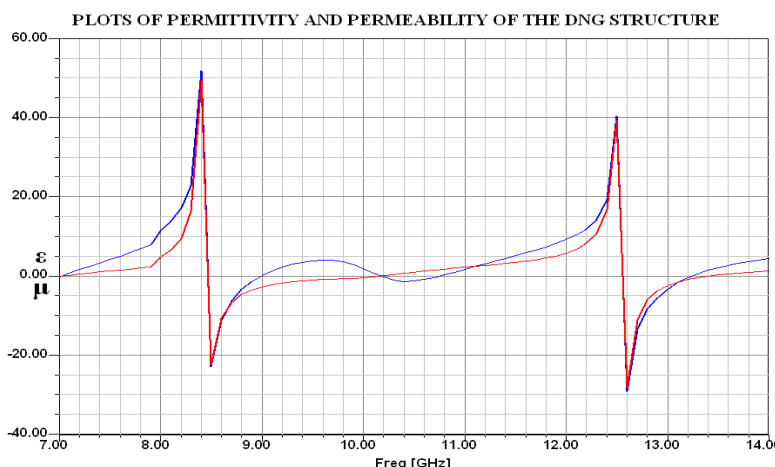


Fig. 11. Effective Permittivity and Permeability of the DNG structure.

After simulating the DNG structure to obtain simultaneous effective negative permittivity and permeability one will be interested to know how the passband characteristics vary with varying various parameters of the DNG structure. The first parameter of interest is the alignment of SRR's and SW's. SW's are rotated in a direction in which they will always remain parallel to the SRR's. The simulation results are provided for  $\theta=0, 45, 90, 135^\circ$  keeping other parameters as constant like  $d'=0.5\text{mm}$ ,  $D=1\text{mm}$ , thickness= $0.01\text{mm}$  and  $\epsilon=3.27$ . The simulation results are shown in Figure 12 (a) to (d).

It is evident that as the SW is moving away from the slits of the SRR there was frequency downshift in the passband characteristics. This can be clearly understood for  $\theta = 0, 45, 90^\circ$ . But as the SW is rotated by  $135^\circ$ , the SW starts moving towards the slits of the SRR and there was a frequency up shift in the passband characteristics when compared to the characteristics for  $\theta = 90^\circ$ . If the SW is closer to the slits of the SRR, than the current flow between the rings of the SRR is reduced because the current starts flowing through the in the same ring though the SW at the slits. This results in a lower value of distributed capacitance which yields a higher resonant frequency. If the SW is away from the slits of the SRR, there will be a larger flow of current between the two concentric rings of the SRR resulting in a higher value of distributed capacitance and hence the resonant frequency is lower when compared to the case where the SW is closer to the slits of the SRR.

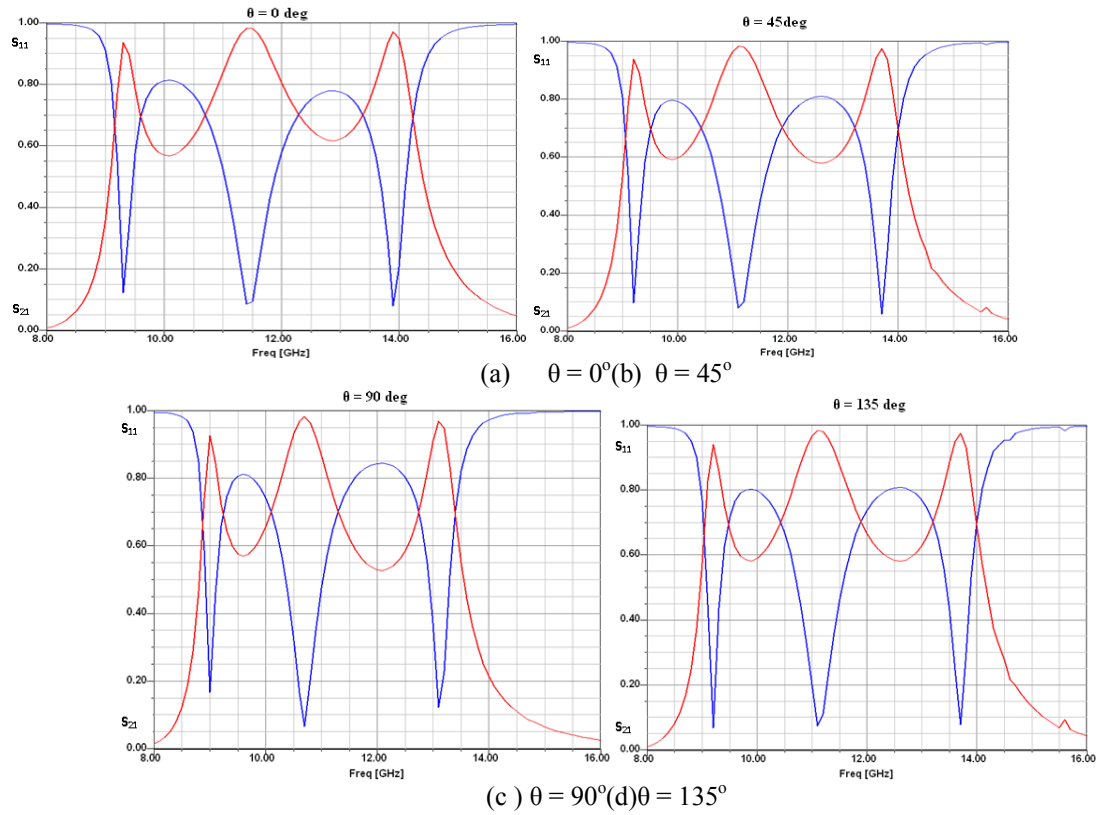


Fig. 12. Variation of  $S_{21}$  with the microwave frequency at the different angle of incidence

The next parameter of interest is the thickness of copper coating used for the design of SRR's and SW's. Keeping  $d'=0.5\text{mm}$ ,  $D=0.5\text{mm}$  and  $\epsilon=2.6$  simulation results are provided for three copper thicknesses  $0.01\text{mm}$ ,  $0.05\text{mm}$  and  $0.1\text{mm}$ . Their investigated results are shown in Figure 13(a) to (d). By observing the characteristics in all the cases it is evident that there was a frequency upshift in the passband characteristics as we increase the copper thickness. This upshift in the passband characteristics is due to the change in the capacitance and inductance values of the DNG structure.

The dielectric constant of the dielectric used for the design of DNG structure affects the passband characteristics. The dielectric constant is varied from 2 to 17 keeping other parameters at  $d'=0.5\text{mm}$ ,  $D=0.5\text{mm}$ ,  $Th=0.01\text{mm}$  are constant. From the simulated results one can observe two prominent effects which is shown in Figure 14 (a) to (e). First one is that there was a frequency downshift in the pass band characteristics with an increase in dielectric constant and the second one is that the width of the passband goes on decreasing with an increase in the dielectric constant of the dielectric. As capacitance is directly proportional to the permittivity of the medium the passband characteristics shift downward with an increase in the permittivity of the DNG structure.

Distance between two SRR structures also plays an important factor. To know how the distance between two SRR's effects the passband characteristics one has to keep all parameters constant and vary the distance between two SRR's. Here the parameters are fixed as  $d'=0.5\text{ mm}$ , Thickness =  $0.01\text{ mm}$  and  $\epsilon=3.27$ . We vary the distance between SRR's from  $1\text{ mm}$  to  $5\text{ mm}$  and observe its effect. The simulated results are shown in Figure 15 (a) to (d) . From the results, it could be observed that there was frequency downshift in passband characteristics with increasing distance. It could also observed that the passband is becoming narrower. Also the distortion in the passband gets increased when we increase the distance between the SRR's. The distortion is so high that almost the passband is vanished.

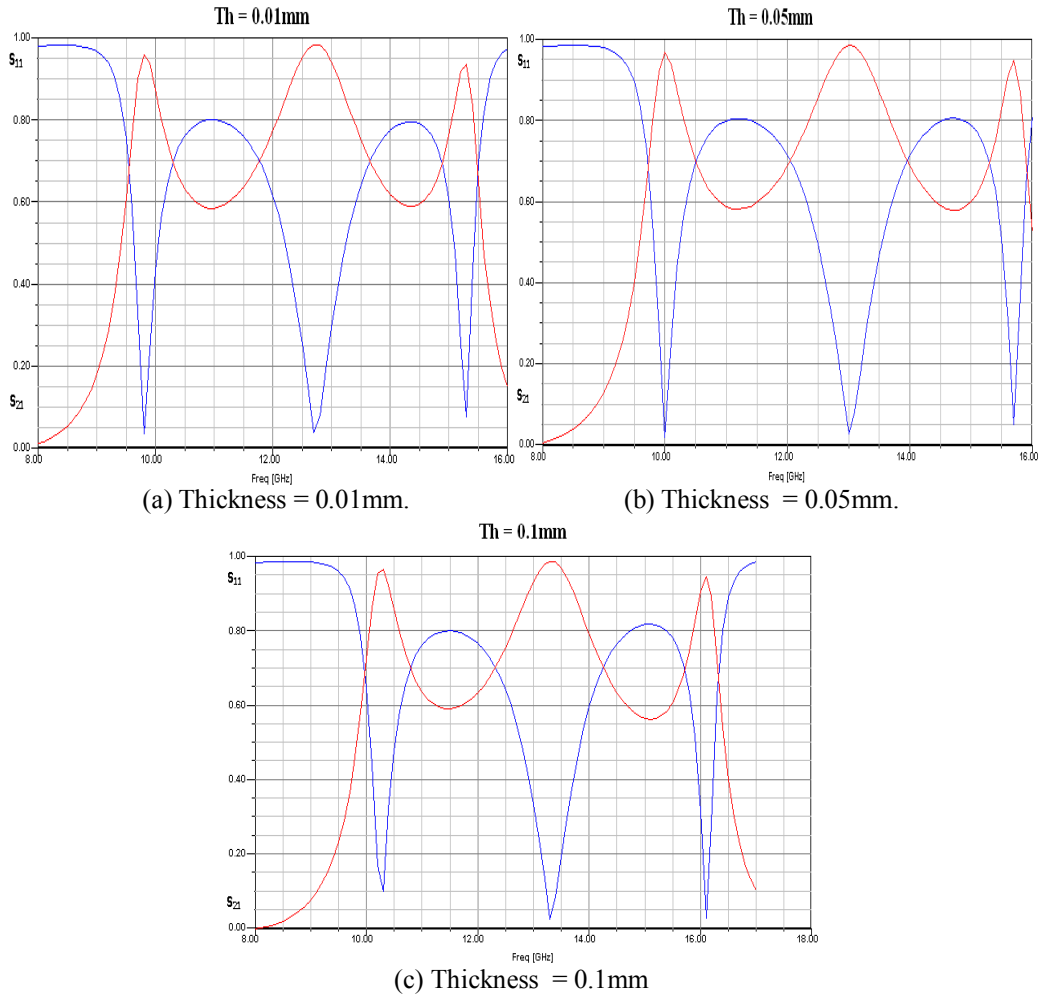
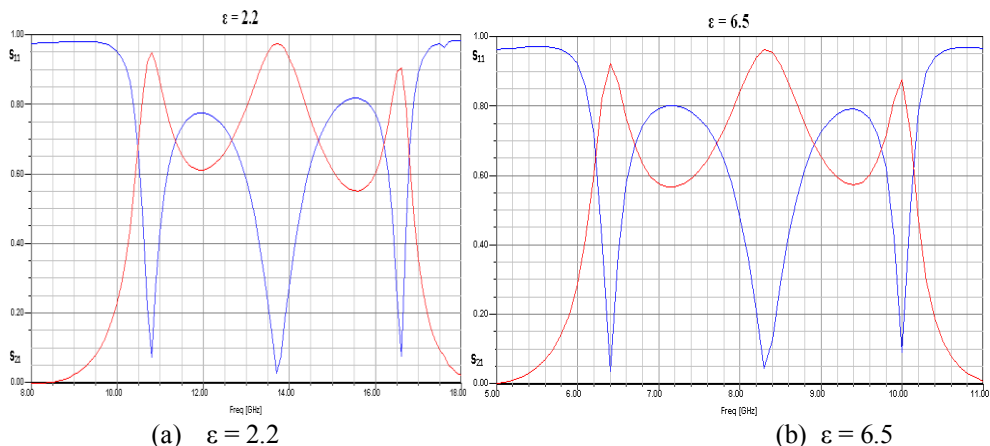


Fig. 13. Variation of  $S_{21}$  with the applied frequency at the different thickness of the copper

The distance between the SRR's and SW's i.e. the thickness of the dielectric also affects the characteristics of the pass band. To study how the pass band characteristics change we have taken  $D=0.5\text{mm}$ ,  $\text{Th}=0.01\text{mm}$ ,  $\epsilon=2.6$  and varied the distance between SRR's and SW's ( $d'$ ). Here we simulate the passband characteristics for two distances 0.5mm and 0.75mm. The simulated results are shown Figure 16 (a) and (b) . From the results we observe that there was a slight frequency upshift with an increase in the distance between SRR's and SW's.



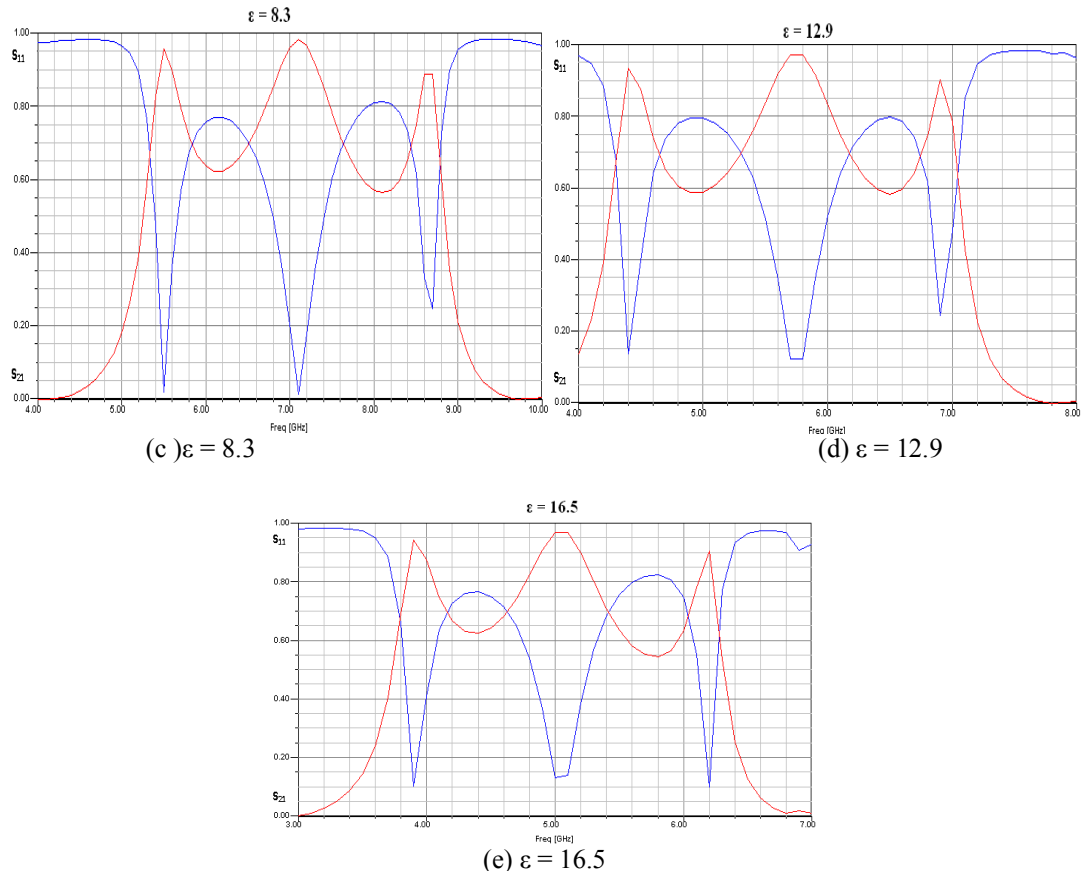


Fig. 14. Variation of the  $S_{21}$  with applied frequency at different dielectric constant

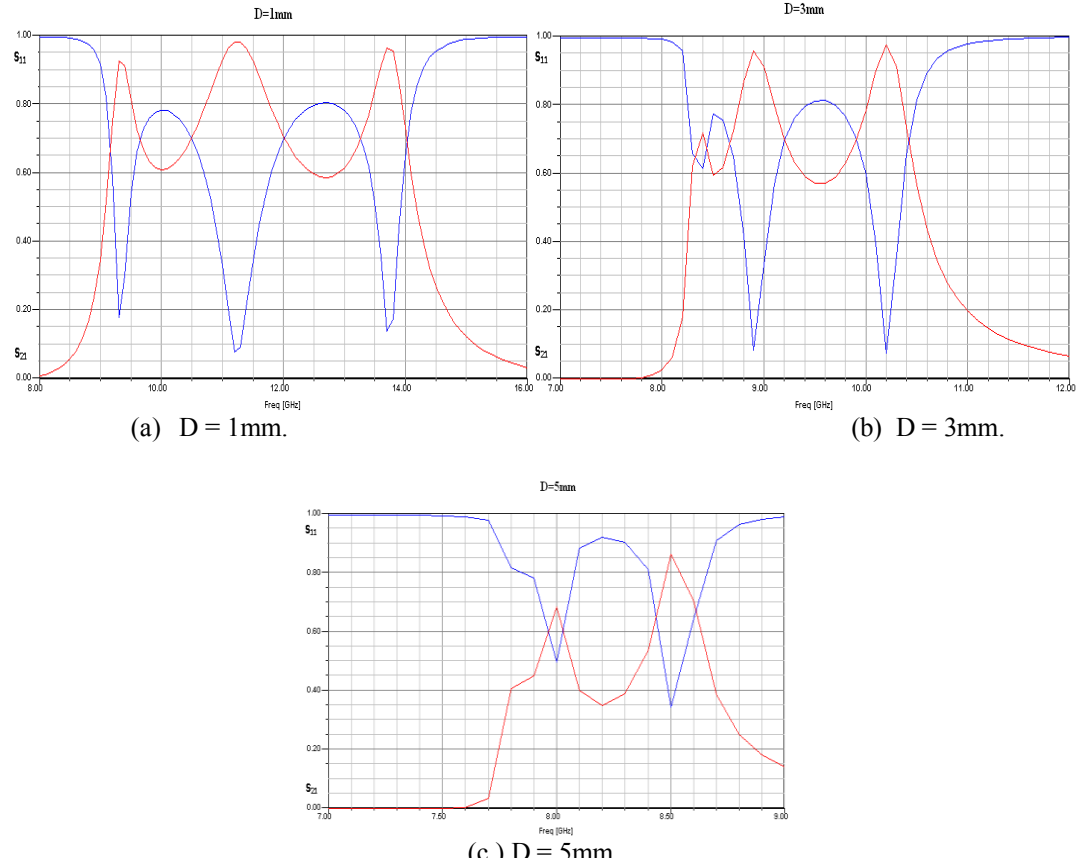


Fig. 15. Variation of  $S_{21}$  with applied frequency at different SRR distance

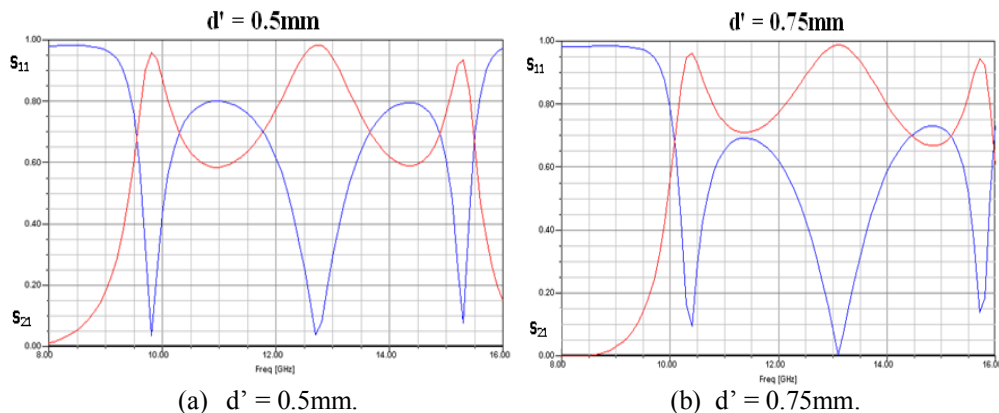


Fig.16.Variation of  $S_{21}$  with applied frequency at different distance between SRR and SW

After studying the effect of various parameters on the passband characteristics of the DNG structure the next step is to observe how the DNG structure affects the characteristics of the horn antenna. The horn antenna without the DNG structure is simulated and the horn antenna characteristics are noted. After this step simulation of the combination of horn antenna and DNG structure is carried out and the characteristics of the combination are noted. By comparing these two cases we could clearly observe the effect of DNG on the horn antenna.

At 8.5 GHz frequency, where simultaneous negative permittivity and permeability are obtained the antenna characteristics with and without DNG structure are given in Table1. From the table it is evident that the directive gain of the antenna increases when the combination of antenna and DNG structure is used. This proves that the DNG structure has the ability to congregate energy.

TABLE1. Antenna characteristics at 8.5 GHz frequency

Paramter	Without DNG	With DNG
Max U	2.4595	2.3227
Peak Directivity	28.568	28.817
Peak Gain	30.997	29.237
Peak Realized Gain	30.907	29.189
Radiated power	1.0819	1.0129
Accepted power	0.9971	0.99835
Incident Power	1	1
Radiation Efficiency	1.085	1.0146
Decay Factor	0	0

At 10 GHz frequencies, where the DNG structure acts as an ordinary structure with positive permittivity and permeability, the antenna characteristics are given in Table 2. From the table it is evident that the directive gain of the antenna decreases when the horn antenna is simulated along with the DNG structure. This is because some of the radiation is blocked by structure from reaching the receiver.

TABLE 2.Antenna Parameters at 10 GHz frequency.

Parameter	Without DNG	With DNG
Max U	3.4882	3.2252
Peak Directivity	40.18	40.131
Peak Gain	43.948	40.662
Peak Realized Gain	43.835	40.53
Radiated power	1.091	1.0099
Accepted power	0.99744	0.99677
Incident Power	1	1
Radiation Efficiency	1.0938	1.0132
Decay Factor	0	0

After obtaining the antenna characteristics with and without DNG structure through simulation, testing of the fabricated DNG structure is carried out in the Laboratory. The E – Plane, H – Plane patterns for Co and

Cross polarizations at 8.5 GHz and 10 GHz are measured. The information regarding the gains of the antenna with and without DNG structure is given in Table 3. From the table one could observe that the DNG structure causes an increase in the gain of the antenna in the DNG range and a decrease in gain when the frequency is not in the DNG range. The H – Plane radiation patterns at 8.5 GHz (both co-polar and cross polar) are as shown in Figure 17. Various parameters like peak relative gain, 3 dB beamwidth, first side-lobe level and cross polarization level for the radiation characteristics are given in Table 4.

TABLE 3. Gain information of horn antenna with and without DNG at 8.5 GHz and 10 GHz.

Parameter	8.5GHZ	10GHz
$\lambda$	3.5294cm	3cm
Gain of Standard antenna	35.086	48.562
Gain of Test antenna without DNG	39.2629	53.56
Gain of Test antenna with DNG	42.2751	42.8488

TABLE 4. H – Plane characteristics with and without DNG structure.

Parameter	Without DNG	With DNG
Maximum relative Gain (dB)	-0.52178	0
Half Power Beam Width	20°	16°
First Side lobe Level (dB)	-19 dB	-20
Relative Cross Polarization level (dB)	-17.6049	-16.037

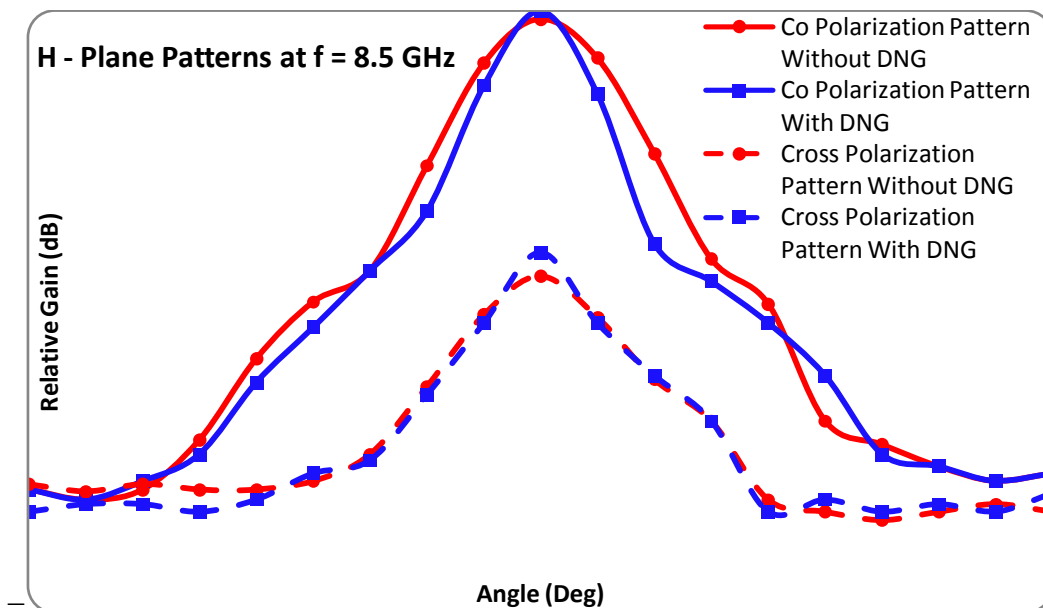


Fig. 17.H- Plane patterns at 8.5 GHz frequency

The E – Plane radiation patterns at 8.5 GHz (both co-polar and cross polar) are as shown in Figure 18. Various parameters like peak relative gain, 3 dB beamwidth, first sidelobe level and cross polarization level for the radiation characteristics are given in Table 5.

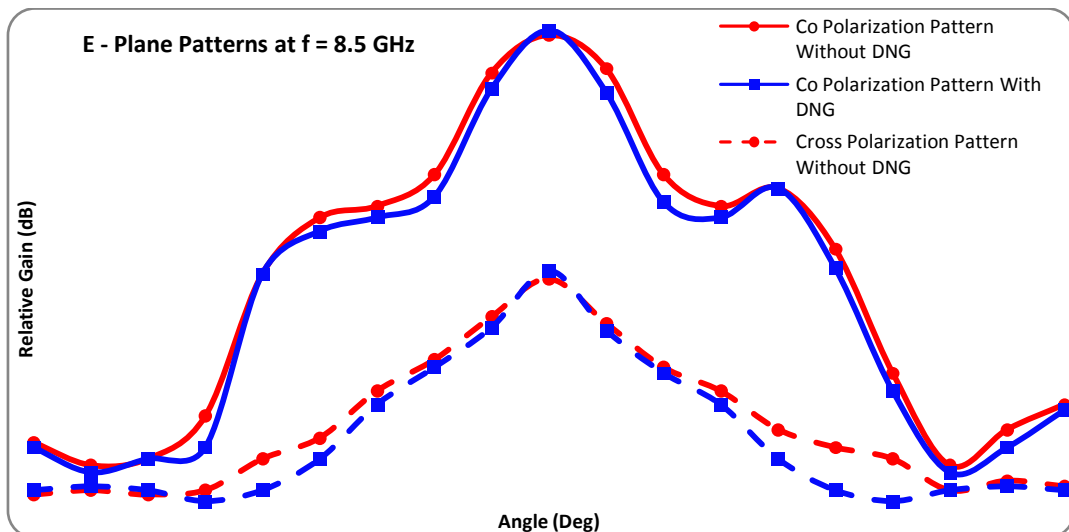


Fig. 18. E – Plane patterns at 8.5 GHz frequency

TABLE 5. E – Plane characteristics with and without DNG structure

Parameter	Without DNG	With DNG
Maximum relative Gain (dB)	0	-0.9691
Half Power Beam Width	22 °	20 °
First Side lobe Level (dB)	-19	-18
Relative Cross Polarization level (dB)	-15.7403	-16.2464

It could be observed from the above information that the gain of the horn antenna increases in the presence of DNG structure and the half power beamwidth as well as the first sidelobe levels are decreased which implies that the antenna is more directive with the presence of the DNG structure at 8.5 GHz. But the disadvantage with the DNG structure is that we are getting an increase in the cross polarization levels at 8.5 GHz.

The H – Plane radiation patterns at 10 GHz (both copolar and cross polar) are as shown in Figure 19. Various parameters like peak relative gain, 3 – dB beamwidth, first sidelobe level and cross polarization level for the radiation characteristics are given in Table:6. The E – Plane radiation patterns at 10 GHz (both copolar and cross polar) are as shown in Figure 20. Various parameters like peak relative gain, 3 – dB beam width, first side lobe level and cross polarization level for the radiation characteristics are given in Table: 7.

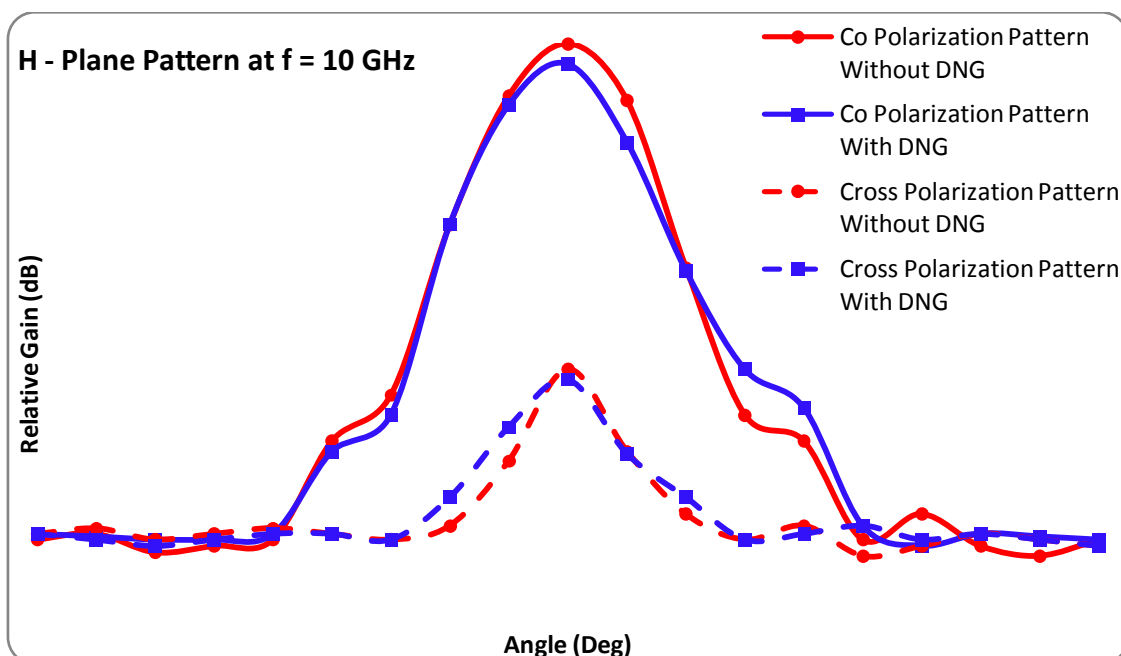


Fig.19.H – Plane patterns at 10 GHz frequency

TABLE 6. H – Plane characteristics with and without DNG structure

Parameter	Without DNG	With DNG
Maximum relative Gain (dB)	-0.34762	0
Half Power Beam Width	17 °	14 °
First Side lobe Level (dB)	-13	-14
Relative Cross Polarization level (dB)	-17.5222	-16.9481

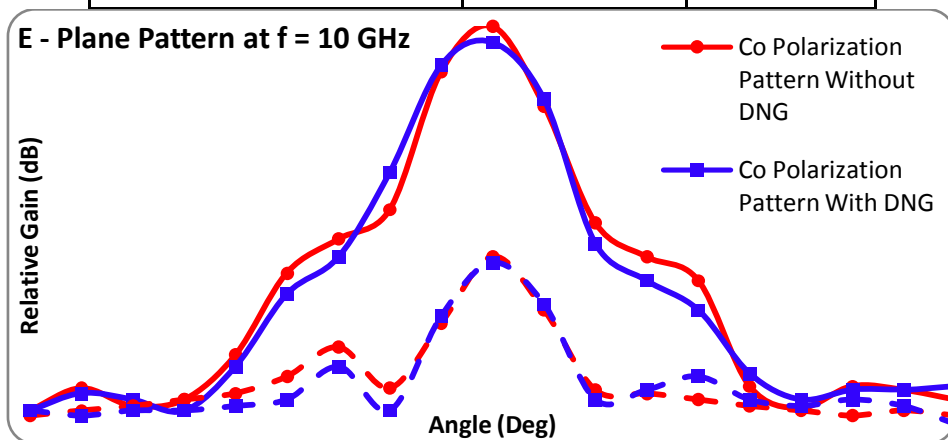


Fig. 20.E – Plane patterns at 10 GHz frequency

Table7. E – characteristics and without structure

Plane with DNG

Parameter	Without DNG	With DNG
Maximum relative Gain (dB)	0	-0.9691
Half Power Beam Width (dB)	18°	20°
First Side lobe Level (dB)	-15	-16

It could be observed from the above information that the gain of the horn antenna decreases in the presence of DNG structure at 10 GHz because the DNG structure acts as an ordinary DPS material at this frequency. The half power beamwidth increases, the first sidelobe levels are decreased which indicates that the antenna is becoming less directive in the presence of the DNG structure at 10 GHz. The cross polarization levels decrease in the presence of DNG structure at 10 GHz frequency.

The input VSWR of the horn antenna with and without the DNG structure is measured and the results are as shown in Figure 21. At 8.5 GHz the difference between the two curves is more because the reflected power from the DNG structure gets congregated because of the DNG effect and the antenna receives more reflected power at this frequency.

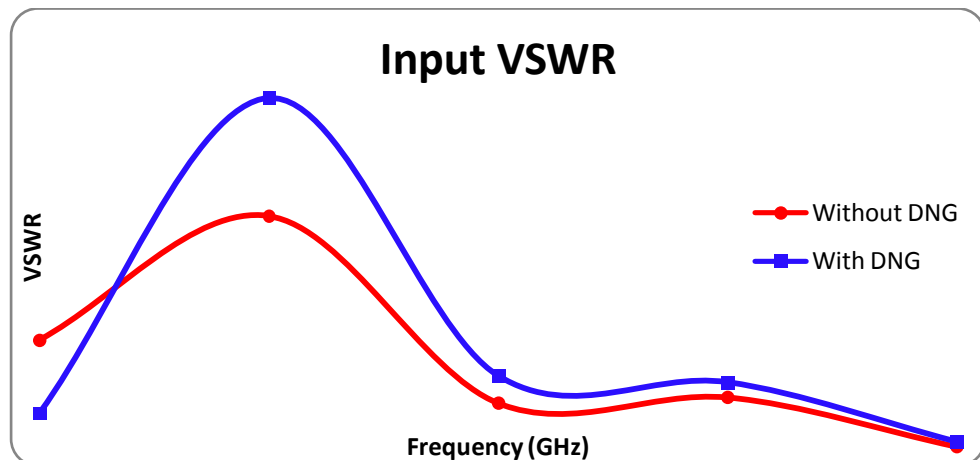


Fig. 21. Input VSWR with and without DNG structure.

## V. Conclusion

- At 8.5 GHz where the Double Negative Structure gives simultaneous negative permittivity and permeability, an improvement in the radiation characteristics of the horn antenna is observed.
- An improvement in the gain of the horn antenna and a decrease in its 3-dB beamwidth has been obtained at 8.5 GHz. The sidelobe level decreases and an increment in the cross-polarization level have been obtained at 8.5 GHz in the presence of Double Negative Structure. It has been verified both by simulation and testing that the horn antenna becomes more directive in the presence of the Double Negative Structure.
- At 10 GHz frequencies where the Double Negative Structure behaves as an ordinary Double Positive Structure, decrease in the gain of the horn antenna is obtained. An increment in 3-dB beamwidth along with a decrease in sidelobe level and cross polarized level has been obtained at 10 GHz. The input VSWR increases in the presence of Double Negative Structure at both 8.5 GHz and 10GHz.
- DNG structure can be made on different dielectric substrates and the difference between the two structures can be studied. Different types of resonator structures can be used instead of Split Ring Resonators to obtain negative permeability. An array of infinitesimally small metallic spheres can be used instead of an array of Strip Wires to produce negative permittivity.

## Reference

- [1] Love, A. W., "Electromagnetic Horn Antenna", IEEE Press, New York, 1976.
- [2] Stutzman, W. L. and G. A. Thiele, "Antenna Theory and Design", 2nd edition, John Wiley & Sons, 1998.
- [3] Balanis, C. A., "Antenna Theory Analysis and Design", 3rd edition, John Wiley & Sons, New Jersey, 2005.
- [4] Bird, T. S. and A. W. Love, "Horn antennas," *Antenna Engineering Handbook*, 4th edition, 14-1-14-74, J. Volakis (ed.), McGraw-Hill, 2007.
- [5] W. E., "Metal-lens antennas," *Proceedings of the IRE*, Vol. 34, 828{836, 1946.
- [6] Chatterjee, R., "Antenna Theory and Practice", 2nd edition, New Age International, 1996.
- [7] R. S., "Antenna Theory and Design", Revised edition, John Wiley & Sons, 2003.
- [8] Lier, E. and R. Landes, "High gain linearly polarised dual band horn for multi-feed reflector antenna," *Electronics Letters*, Vol. 39,1230 -1232, 2003.
- [9] Tsandoulas, G. and W. Fitzgerald, "Aperture efficiency enhancement in dielectrically loaded horns," *IEEE Transactions on Antennas and Propagation*, Vol. 20, 69-74, 1972.
- [10] Hui, W. W. G., J. M. Bell, M. F. Iskander, and J. J. Lee, "Low-cost microstrip-line-based ferritephase shifter design for phased array antenna applications," *IEEE Antennas and Wireless Propagation Letters*, Vol. 6, 86{89, 2007.
- [11] Ikram, S. and G. ahmad, "Design & implementation of a standard gain horn antenna for optimized gain and radiation pattern using math-CAD & HFSS," *Second International Conference on Electrical Engineering*, University of Engineering and Technology, Lahore, Pakistan, March 25-26, 2008.
- [12] Luo, G. Q., W. Hong, H. J. Tang, J. X. Chen, X. X. Yin, Z. Q. Kuai, and K. Wu, "Filtenna consisting of horn antenna and substrate integrated waveguide cavity FSS," *IEEE Transactionson Antennas and Propagation*, Vol. 55, No. 1, 92-98, January 2007.
- [13] Yin, X.-C., C.-L. Ruan, S.-G. Mo, C.-Y. Ding, and J.-H. Chu, "A compact ultra-wideband microstrip antenna with multipole notches," *Progress In Electromagnetics Research*, Vol. 84, 321-332, 2008.
- [14] Venkatayalu, N. V., C.-C. Chen, F. L. Teixeira, and R. Lee, "Numerical modeling of ultrawide-band dielectric horn antennas using FDTD," *IEEE Transactions on Antennas and Propagation*, Vol. 52, No. 5, 1318-1323, May 2004.
- [15] N. Engheta, R.W. Ziolkowski, Eds., Metamaterials: Physics and Engineering Explorations, Wiley-IEEE Press, Hoboken, NJ, 2006.
- [16] Veselago, V. G., The electrodynamics of substances with simultaneously negative values of permittivity and permeability, Sov. Phys. Usp., 1968, 10(4): 509-514.
- [17] Houck, A. A., Brock, J. B., Chuang, I. L., Experimental observation of a left-handed material that obeys Snell's law, *Phys. Rev. Lett.*, 2003, 90(13): 137401-137408.
- [18] Seddon, N., Bearpark, T., Observation of the inverse Doppler effect, *Science*, 2003, 302(5650): 1537-1540.

- [20] Pendry, J. B., Negative refraction makes a perfect lens, *Phys. Rev. Lett.*, 2000, 85(18): 3966-3969.
- [21] R.W. Ziolkowski, A. Kipple, "Application of double negative metamaterials to increase the power radiated by electrically small antennas," *IEEE Trans. Antennas Propag.*, Vol. 51, pp. 2626-2640, 2003.
- [22] R.W. Ziolkowski, A.D. Kipple, "Reciprocity between the effects of resonant scattering and enhanced radiated power by electrically small antennas in the presence of nested metamaterial shells," *Phys. Rev. E*, Vol. 72, 036602, 2005.
- [23] X. Chen, T.M. Grzegorczyk, B.-I. Wu, J. Pacheco, Jr., J.A. Kong, *Phys. Rev. E* 70, 016608 (2004).
- [24] D.R. Smith, J.B. Pendry, *J. Opt. Soc. Am. B* 23, 391 (2006).
- [25] M. Davanco, Y. Urzhumov, G. Shvets, *Opt. Express* 15, 9681 (2007).
- [26] T. Driscoll, D.N. Basov, W.J. Padilla, J.J. Mock, D.R. Smith, *Phys. Rev. B* 75, 115114 (2007).
- [27] C. Menzel, C. Rockstuhl, T. Paul, F. Lederer, *Phys. Rev. B* 77, 195328 (2008).
- [28] C. Menzel, T. Paul, C. Rockstuhl, F. Lederer, T. Pertsch, S. Tretyakov, arXiv:0908.2393[physics.optics] (2009).
- [29] Lin, H.-H., C.-Y. Wu, and S.-H. Yeh, 'Metamaterial enhanced high gain antenna for WiMAX application,' *IEEE AP-S*, Oct. 2007.
- [30] Russo, P., R. Rudduck, and L. Peters, Jr., 'A method for computing E-plane patterns of horn antennas,' *IEEE Trans. Antennas and Propagation*, Vol. 13, No. 2, 219-224, Mar. 1965.
- [31] Safaai-Jazi, A. and E. Jull, 'A short horn with high E-plane directivity,' *IEEE Trans. Antennas and Propagation*, Vol. 25, No. 6, 854-859, Nov. 1977.
- [32] Yu, J., R. Rudduck, and L. Peters, Jr., 'Comprehensive analysis for E-plane of horn antennas by edge diffraction theory,' *IEEE Trans. Antennas and Propagation*, Vol. 14, No. 2, 138-149, Mar. 1966.
- [33] Rhodes, D. R., 'An experimental investigation of the radiation patterns of electromagnetic horn antennas,' *Proceedings of the IRE*, Vol. 36, No. 9, 1101-1105, Sept. 1948.
- [34] Jull, E., 'Errors in the predicted gain of pyramidal horns,' *IEEE Trans. Antennas and Propagation*, Vol. 21, No. 1, 25-31, Jan. 1973.
- [35] Jull, E., 'Reflection from the aperture of a long E-plane sectoral horn,' *IEEE Trans. Antennas and Propagation*, Vol. 20, No. 1, 62-68, Jan. 1972.
- [36] Liu, K., C. A. Balanis, C. R. Birtcher, and G. C. Barber, 'Analysis of pyramidal horn antennas using moment methods,' *IEEE Trans. Antennas and Propagation*, Vol. 41, No. 10, 1379-1389, Oct. 1993.
- [37] Gupta, R. C., 'Analysis of radiation patterns of compound boxhorn antenna,' *Progress In Electromagnetics Research*, PIER 76, 31-34, 2007.